Floating Coil Position Detection System for the Levitated Dipole Experiment

by

Austin Hayes Roach

Submitted to the Department of Physics
in partial fulfillment of the requirements for the degree of

Bachelor of Science in Physics

at the

MASSACHUSETTS INSTITUTE OF TECHNOLOGY

June 2005

Author .....
Department of Physics
May 17, 2005

Certified by .....
Darren Garnier
Research Scientist, Columbia University
Thesis Supervisor

Read by .....
Ronald Parker
Professor of Nuclear Science and Engineering
Thesis Reader

Accepted by .....
Professor David E. Pritchard
Senior Thesis Coordinator, Department of Physics

Floating Coil Position Detection System for the Levitated Dipole Experiment

by

Austin Hayes Roach

Submitted to the Department of Physics
on May 17, 2005, in partial fulfillment of the
requirements for the degree of
Bachelor of Science in Physics

Abstract

The Levitated Dipole Experiment (LDX) is a joint Columbia University/MIT research collaboration sited at MIT's Plasma Science and Fusion Center. LDX is investigating the physics of a plasma confined in a dipole magnetic field. The field is created with a superconducting electromagnetic ring in the center of a large vacuum chamber. The goals of the experiment call for the ring to be levitated in the center of the vacuum vessel by the magnetic field of another superconducting electromagnet. This act requires a feedback mechanism to control the position of the ring in the vacuum vessel. This thesis presents a design for a position detection system to give position information to the feedback controller and digital filters to reduce the effect of noise in the position measurements.

Thesis Supervisor: Darren Garnier
Title: Research Scientist, Columbia University

Acknowledgments

It is my pleasure to thank all of the people who helped me as I wrote this thesis.

I cannot adequately show my appreciation for my thesis advisor, Dr. Darren Garnier. He has taught me an incredible amount over the several years that I have worked with him, and without his help, encouragement, and clear explanations, I could not have written this thesis.

Thanks also to everyone on the LDX team who provided me with help when I needed it and who took the time to explain things to a curious undergraduate. LDX taught me a lot about experimental plasma physics, and I am thankful to everyone who helped me learn.

I would also like to thank all of the people at La Maison Française who provided me with friendship, humor, and good conversation throughout my undergraduate years.

Finally, I would like to thank my family. My parents, Charles and Brenda, and my brother Keith have given me unrelenting love and support during my time at MIT. Without them, none of this would have been possible. Thank you.

Contents

List of Figures

Chapter 1

Introduction

1.1 Introduction to the Levitated Dipole Experiment

The Levitated Dipole Experiment (LDX) is a research project at MIT's Plasma Science and Fusion Center that is investigating a novel approach to magnetic plasma confinement. LDX allows scientists to study the physics of plasma in a dipole magnetic field similar to those produced by the magnetospheres of planets such as Jupiter[1]. Results from the Voyager spacecraft and theoretical calculations have suggested that a dipole magnetic field could have characteristics desirable in a nuclear fusion device, such as high β equilibrium, near classical energy confinement, convective cell formation, and a simplified magnet geometry[1, 2, 3]. LDX is investigating the physics of plasmas confined in such magnetic fields in order to determine the validity of these theories.

The core of the experiment is a set of three superconducting electromagnets and a large, 5-meter diameter vacuum vessel as shown in Figure 1-1. The first magnet is the Floating coil, or F-coil. This is the magnet responsible for making the dipole-like field for which the experiment is named, and is, as the name suggests, capable of floating in the center of the vacuum vessel. The second coil is the Levitation coil, or L-coil. The L-coil is positioned atop the vacuum vessel and creates a magnetic field that

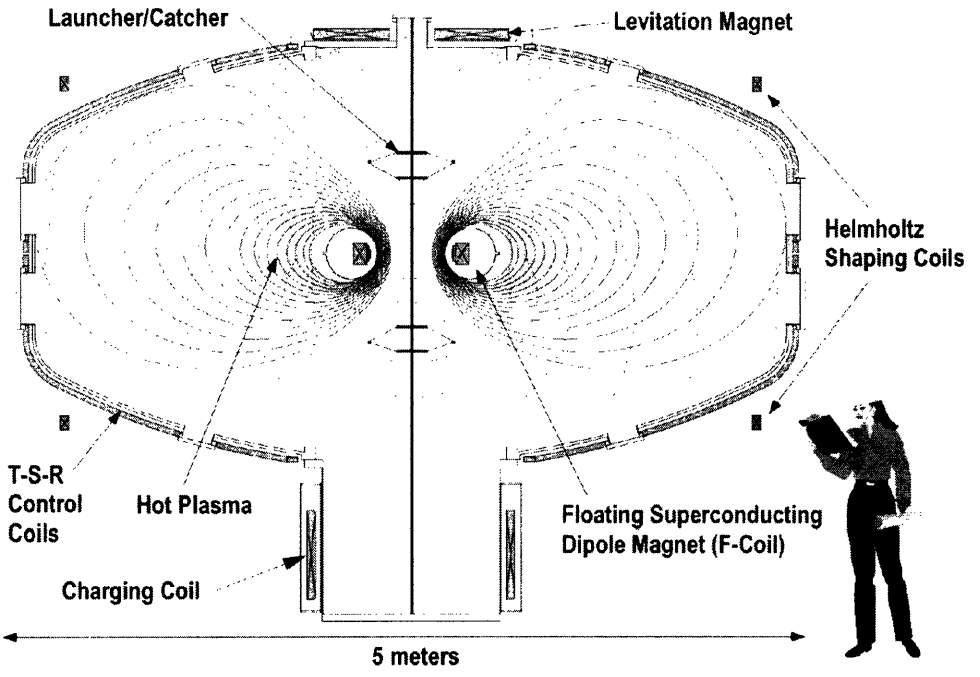

Figure 1-1: A side view of the Levitated Dipole Experiment is shown. The F-coil, which is levitated in the center of the vacuum chamber, is attracted from above by the L-coil to balance the force of gravity.

attracts the F-coil from above. This counterbalances the force of gravity, allowing the F-coil to float in the center of the vacuum chamber. The final superconducting electromagnet is the Charging coil, or C-coil. The C-coil is used to inductively charge the F-coil.

LDX began experimental operations in August of 2004, and has performed several successful experimental runs since that time. As of the writing of this thesis, LDX has operated only with a supported F-coil, meaning that the F-coil is held physically in place by the launcher/catcher system. These supports cause plasma losses, and because of this, the physics goals of the experiment ultimately demand that the machine operate with the F-coil freely floating in the center of the vacuum vessel. So, we are posed with the problem of how to levitate a 600 kg superconducting electromagnet in the center of a 5 meter diameter vacuum vessel.

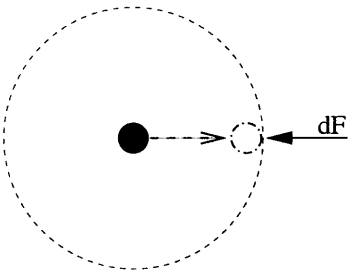

Figure 1-2: Small displacement of an object from an equilibrium point to a point on an imaginary surface. The force on the object at that point is restoring and pushes the object back to its equilibrium position.

1.2 Earnshaw's Theorem

Earnshaw showed in a paper in 1842 that there is no stable arrangement of a finite number of static electric charges [4]. This result is known as Earnshaw's Theorem. Although Earnshaw proved his original theorem for electric charges, the result can be generalized to a static arrangement of any forces obeying an inverse square force law.

The proof of Earnshaw's theorem rests on the divergencelessness of inverse square law force fields. Consider an object in an equilibrium as shown in Figure 1-2. The object is displaced to the edge of an imaginary closed surface, and the force on the object at that point is considered. If the force is a restoring force, the force must point back in the direction of the equilibrium position and is a stabilizing force as shown in Figure 1-2. If, however, the force vector points away from the equilibrium position as in Figure 1-3, the force is a destabilizing force and is indicative of an unstable equilibrium.

The forces on the object can be evaluated for small displacements of the object from the equilibrium position to each point on the imaginary surface. If all of the forces point inward, this indicates that the equilibrium is a stable one. This also implies that there is a divergence of the force in the volume enclosed by the imaginary surface. So, if there exists a stable equilibrium for the object, there must be a point where the divergence of the force field is non-zero.

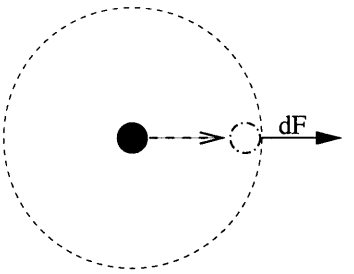

Figure 1-3: Small displacement of an object from an equilibrium point to a point on an imaginary surface. The force on the object at that point accelerates the object away from the equilibrium point, indicating an unstable equilibrium.

The force for any inverse square law force is given by

$$\vec{F} = \frac{A\hat{r}}{r^2} \tag{1.1}$$

where A is some constant which is characteristic of the physics of the force. The divergence of such a force is given by

$$\vec{\nabla} \cdot \vec{F} = \frac{1}{r^2}\frac{\partial}{\partial r}(r^2 \cdot \frac{A\hat{r}}{r^2}) = \frac{1}{r^2}\frac{\partial}{\partial r}(A\hat{r}) = 0 \tag{1.2}$$

We see that the divergence of an inverse square law force is zero in a volume of space not containing the source of the force. This means that the force vectors into a region cannot all point into the interior, since such an arrangement would imply a non-zero divergence. There must be some force vectors pointing out of our imaginary surface if any force vectors point in. This implies that the equilibrium is unstable.

In the case of the Floating coil, there will not be one, but several inverse square law forces acting on the coil. The gravitational force acting on the coil behaves as an inverse square law, and the magnetic force acting on the coil also behaves as a sum of small inverse square law forces from each tiny current element of the Levitation coil. So, we want to evaluate the divergence not of a single inverse square law force, but of the sum of a number of such forces, $\vec{F}_{total} = \vec{F}_1 + \vec{F}_2 + \vec{F}_3 + ...$ Evaluating the divergence, we are aided by the fact in vector calculus that the divergence of a sum

is simply the sum of the divergences of the individual components [5]

$$\nabla \cdot \vec{F}_{total} = \nabla \cdot (\vec{F}_1 + \vec{F}_2 + \vec{F}_3 + ...) = \nabla \cdot \vec{F}_1 + \nabla \cdot \vec{F}_2 + \nabla \cdot \vec{F}_3 + ... = 0 \qquad (1.3)$$

We showed above that the divergence of a single inverse square law force was zero, so we see that the sum of such forces also has a divergenceless field of force, again implying that there is no stable equilibrium.

There are several points where this result breaks down:

- In the case of two inverse square law forces originating at the same point in space and acting with equal and opposite forces, a stable equilibrium does exist. However, this is a trivial result since it is equivalent to no net force being present anywhere in space.
- At a point in space where there is a source of force, there can exist a stable equilibrium if A is negative. In free space, however, the derived result still holds.
- Forces not obeying an inverse square law are not covered by Earnshaw's Theorem.
- Time-varying forces are not covered by Earnshaw's Theorem.

Several systems have been identified that appear on the outset to violate Earnshaw's Theorem, such as diamagnets and precessing ferromagnets that are levitated in magnetic fields [6]. However, careful examination of these systems has shown that the systems have violated at least one of the conditions required for the applicability of Earnshaw's Theorem.

In the case of the F-coil, it is being acted on by inverse square law forces in free space, namely gravity and the force due to its interaction with the magnetic field of the L-coil. So, if it were controlled only with static fields, there must be at least one unstable degree of freedom in its dynamics. This result requires the application of time-varying fields controlled by a feedback mechanism in order to control the F-coil. Time-varying fields are not limited by Earnshaw's Theorem, and are able to produce stable equilibria.

1.3 Need for the Position Detection System

Earnshaw's Theorem showed us that the F-coil must have at least one unstable degree of freedom in the levitated state. There are two obvious magnet configurations for the levitation of another magnet. In one configuration, a magnet is placed below the floating magnet and repels it, canceling the force of gravity. In this configuration, the two slide degrees of freedom and the two tilt degrees of freedom are unstable. But, the vertical translation degree of freedom is stable, and the rotational degree of freedom is metastable. Such a configuration requires feedback to control four degrees of freedom.

In the second configuration, the floating magnet is attracted to another magnet from above. In this configuration, the vertical translation is unstable, but the two degrees of horizontal translation and two degrees of tilt are stable. The rotational degree of freedom is again metastable. This is the configuration chosen for the Levitated Dipole Experiment. In this configuration, feedback is required to control the vertical position of the floating coil. Feedback may also be required to damp oscillations in the other degrees of freedom, since the system itself does not quickly damp oscillations that may arise in those modes.

It is thus necessary to design a position detection system to determine the position of the F-coil in the vacuum chamber in order to give feedback to the levitation system to control the dynamics of the F-coil. The information from the feedback is translated into a time-varying voltage which adds current to the steady DC current of the L-coil in order to account for changes in the position of the floating coil.

1.4 Levitation Control System Design

Figure 1-4 shows a graphical representation of the various components used in the levitation control system. The hub of the activity is a computer with high-speed input/output ports running QNX Neutrino[7], a hard real-time operating system. This system will use the position information from the optical position detection

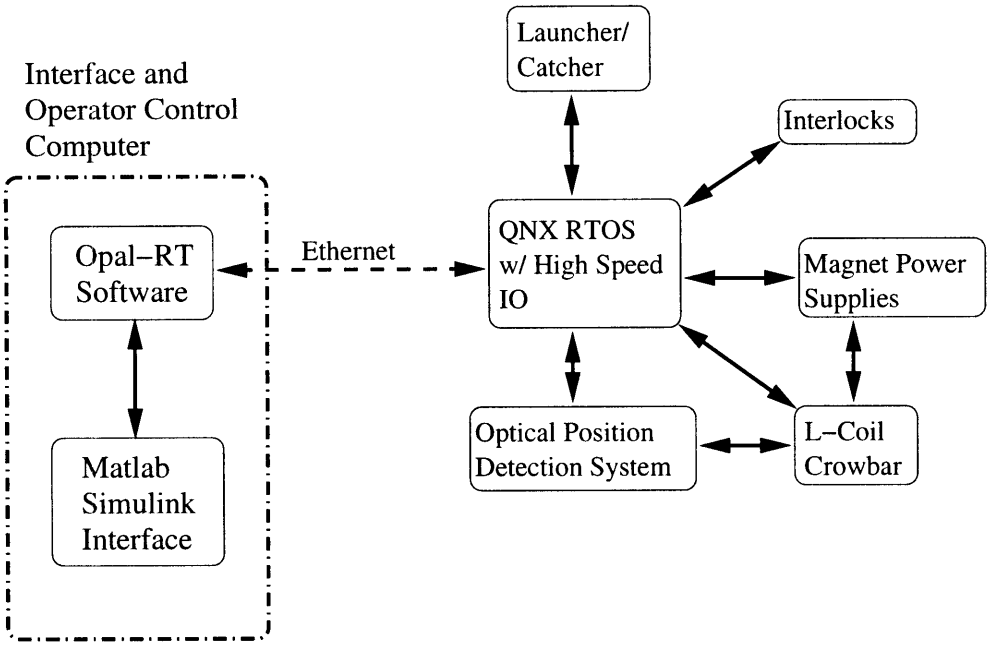

Figure 1-4: Diagram of the interaction of the various components of the digital control system, including the computer running the QNX real-time operating system serving as the hub of the components.

system to provide feedback to the magnet power supplies. It will also be able to control the L-coil crowbar and launcher/catcher in the case of a loss-of-control accident.

The QNX system will be linked to another computer in the control room that will provide operators with the status of the system and will allow them to control some of the feedback parameters. The control system and interface will be designed in MATLAB Simulink[8]. The Simulink model will be translated into C-code by the Opal-RT[9] software and compiled on the QNX machine. The Opal-RT software then serves as a gateway between the MATLAB Simulink control interface and the control computer.

1.5 Organization of the Thesis

Chapter 2 provides information about the floating coil position detection system. It presents the challenge of measuring the position of the floating coil in the the center of the vacuum chamber, and explains how a system was chosen to meet the design

goals of the experiment.

Chapter 3 describes a digital filtering algorithm which could be used to filter the received position signals and to determine the voltage to apply to the levitation coil. Results of the implementation of these filters are shown based on a simple model of the floating coil dynamics.

Chapter 4 presents the conclusions of this thesis and lays out the future work for the development of the floating coil position detection system and the levitation control system.

Chapter 2

Position Detection System Design

The LDX vacuum vessel was designed for a system of throughbeam position detectors, as shown in Figure 2-1. The system consists of eight wide laser beams which pass tangentially to a rim attached onto the F-coil. The rim occludes the laser light in an amount determined by the position of the coil. Two laser beams intersect the rim at each of four points on the rim's surface. At each point of intersection, one laser beam, aligned vertically, is used to measure the vertical position, and the other beam, aligned horizontally, is used to measure the horizontal position as shown in Figure 2-2.

Several design goals for the position detection system were laid out before the beginning of this thesis:

- The system should be immune to the varying light levels produced by the plasma during plasma shots.

- The system should be able to make measurements with a sampling rate of at least 1kHz. This is to ensure measurement faster than the fast modes of oscillation of the system ($\sim$10Hz), resulting in a minimal phase delay in the design of the feedback system.

- The system should be designed to be as resistant to noise as possible, since noise in the system results in unnecessary excitation of the L-coil.

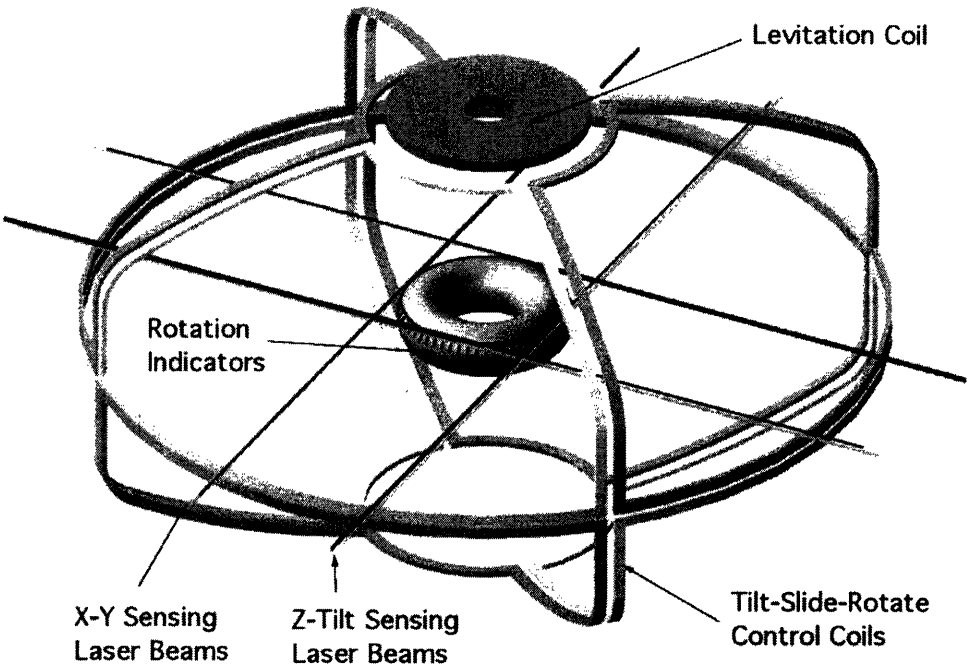

Figure 2-1: Schematic of the laser-beam position detection system showing the Floating coil, the position detection beams passing tangentially to the Floating coil, and the control magnets that will later be installed to damp oscillations in the stable degrees of freedom.

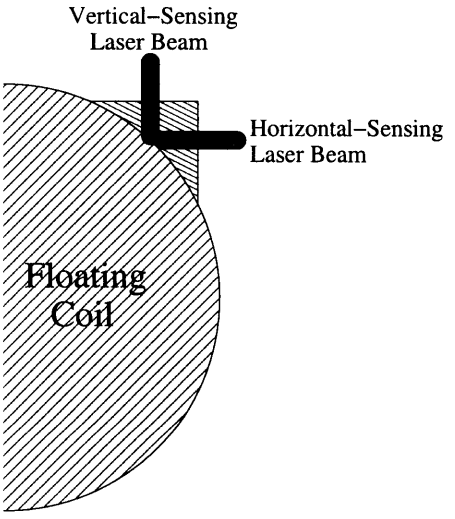

Figure 2-2: Cross-section of the LDX Floating coil and attached rim, showing the intersection of the Position Detection System laser beams with the rim.

The last item is particularly important to the digital filter work presented in Chapter 3. The stabilization of the F-coil is achieved by varying the current in the L-coil, and although the L-coil is superconducting, it does experience heating due to hysteresis losses whenever alternating current is provided [10]. Thus, the heat-removing capacity of the L-coil refrigerator presents a limit on the amount of noise permissible in the system.

2.1 Immunity to Ambient Light

While the LDX vacuum chamber is normally quite dark, the chamber is illuminated significantly during plasma shots. A position detection system that measures the amount of received laser light must not be sensitive to ambient light, since an increase in received light would appear as a change in the F-coil position to the position detection system.

2.1.1 Amplitude Modulated Laser Light

If the output of the laser emitters is at a constant level, the information of the position of the floating coil is carried in the low-frequency amplitude modulation of the received light signal as shown in Figure 2-3. Unfortunately, the plasma itself can be expected to produce abundant quantities of light with an amplitude varying at low frequencies. So, it would be quite difficult to distinguish the information-carrying laser light from the light produced by the plasma.

We can get around the problem of indistinguishable signals if we amplitude modulate the light from the laser emitter. Assuming the laser emitter emits light with the time-varying functional form $A \cdot (0.5 - 0.5\cos(\omega_o t))$, the received signal at the receiver will be of the form

$$g(t) = A \cdot (0.5 - 0.5\cos(\omega_o t)) \cdot f(t) \tag{2.1}$$

where $f(t)$ is the signal produced by the oscillations of the F-coil. We are interested

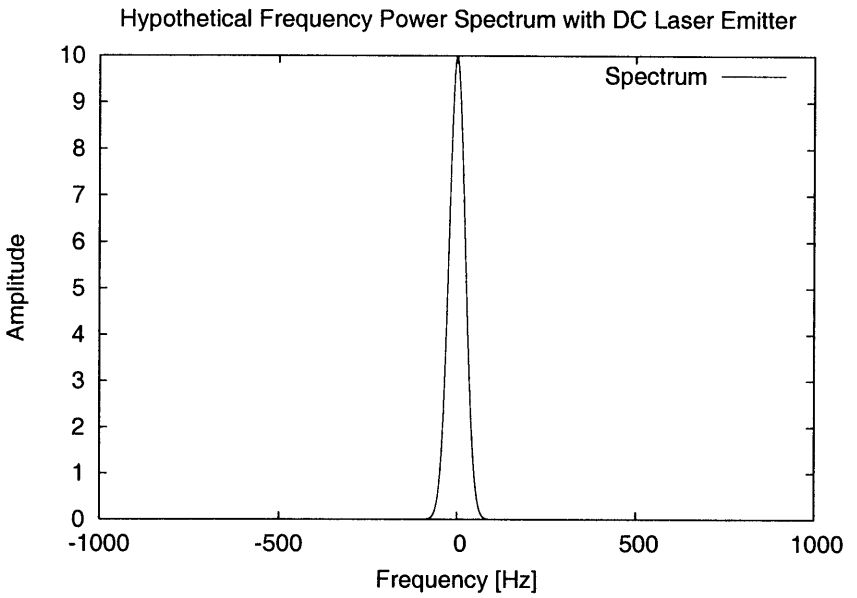

Figure 2-3: Hypothetical frequency spectrum from a measurement based on a constant amplitude laser emitter. The amount of light received is amplitude modulated by the F-coil as it moves inside the vacuum chamber, producing frequency components at the frequency of oscillation of the coil.

in the frequency spectrum of the received signal, so we can take the Fourier transform

$$G(\omega) = \mathcal{F}[g(t)] = \int_{-\infty}^{\infty} e^{-i\omega t} A \cdot (0.5 - 0.5\cos(\omega_o t)) \cdot f(t) dt \tag{2.2}$$

$$\rightarrow G(\omega) = \mathcal{F}[A \cdot (0.5 - 0.5\cos(\omega_o t)] \otimes \mathcal{F}[f(t)] \tag{2.3}$$

$$= A \cdot (0.5[F(\omega)] + 0.25[F(\omega + \omega_o)] + 0.25[F(\omega - \omega_o)]) \tag{2.4}$$

Since it is not possible to center the amplitude modulated light from the laser emitter at a 0 DC level (we cannot emit light with negative power), there is still a considerable fraction of the information's power centered around $\omega = 0$. However, a fraction of the desired signal has been shifted into a region of higher frequency by the amplitude modulated emitter. If we choose an emitter frequency much higher than the frequency components of the light from the plasma, we can distinguish the desired position signal from the noise caused by the ambient light.

The benefits of amplitude modulation have been shown here for a sinusoidal signal, but similar benefits can be gained by pulsing the laser emitter at a high frequency.

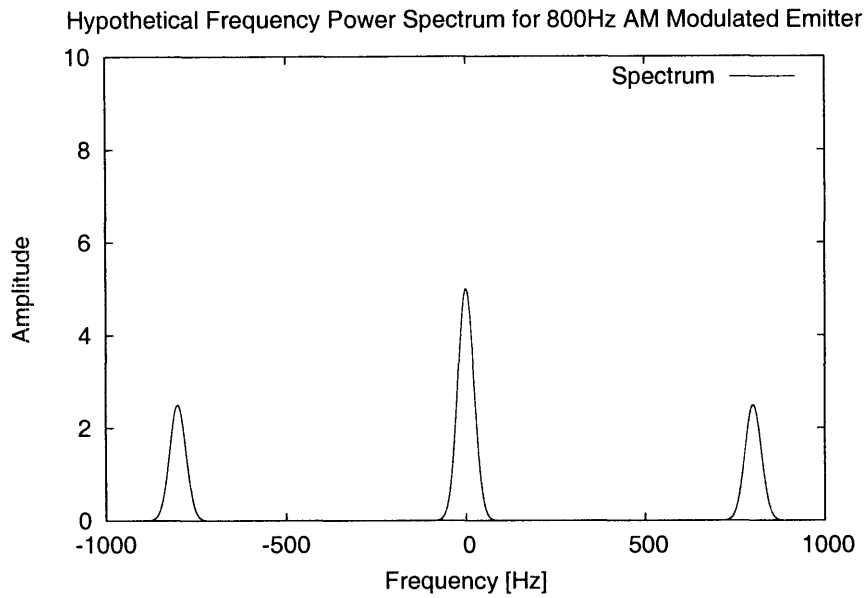

Figure 2-4: Hypothetical frequency spectrum from a measurement based on a laser emitter with a sinusoidally varying output power. A significant portion of the frequency spectrum produced by the F-coil's amplitude modulation is now shifted into a region of higher frequency.

The Fourier transforms of the pulses are somewhat trickier since information will be carried at harmonics of the pulsing frequency, but the same benefits can be gained as by amplitude modulating with a purely sinusoidal signal.

2.1.2 Evaluating the Modulation Frequency

To evaluate the modulation frequency needed in order to overcome the light noise in the system, it is necessary to first evaluate the frequency components produced by the plasma. A photodiode was mounted on one window intended to be used by the position detection system. The photodiode measured the light produced during a plasma shot, and this signal was measured with a sampling rate of ~100kHz. The voltage measured was adjusted for the known efficiency of the detector and the known detector size to give the light power measured in Watts/cm^2. The result is plotted in Figure 2-5.

The expected detector size for the position detector system is on the order of about 1 cm^2, so there is expected to be a total of about 10μW of light power incident

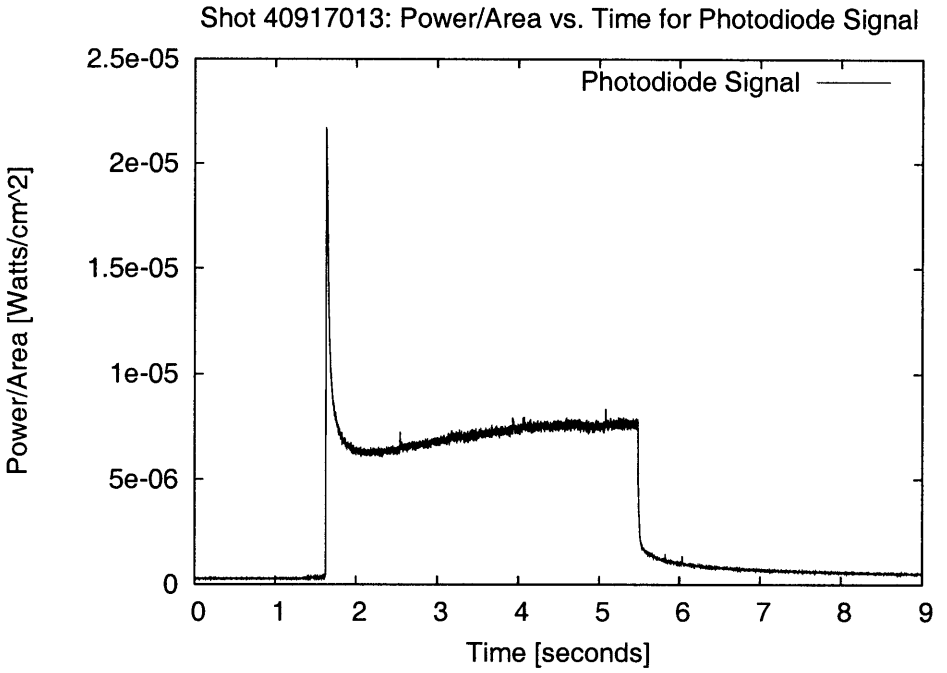

Figure 2-5: Light power during a plasma shot as measured by a photodiode mounted to a window which will later be used for the position detection system. The signal from the photodiode was scaled by the photodiode efficiency and detector area to give a measurement of power per unit area at the wall of the vacuum vessel.

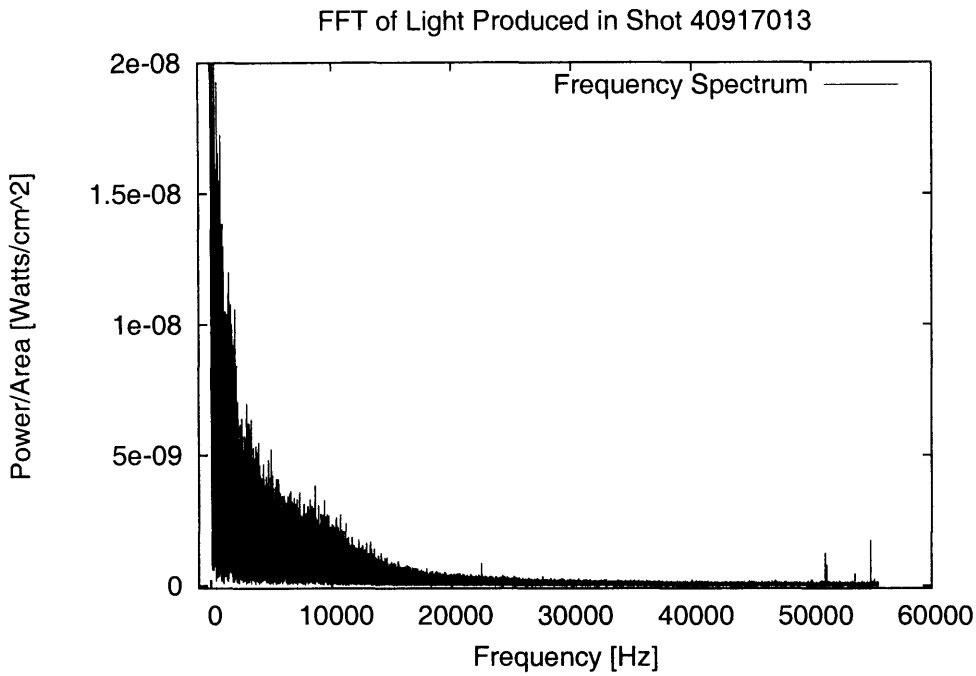

Figure 2-6: Fourier transform of the photodiode signal showing the frequency spectrum. The DC component of the signal is much higher than the other frequency components, on the order of 10^{-5}, and is clipped by the top of the plot.

on the detector. A typical laser diode puts out several milliwatts of power, so the received light from the laser is expected to be a factor of about 100 higher than the light produced by the plasma assuming a large fraction of the emitted laser light is received. If the laser emitter were not modulated, we could expect a signal to noise ratio for the received light to be at most 100:1.

We plan to modulate the laser emitter, so we can evaluate the ambient light spectrum to observe the gains in the signal to noise ratio from amplitude modulating the light from the emitter. This analysis shows how the noise from the plasma light is minimized by amplitude modulating the emitter, but we gain the additional benefit of being immune to other sources of low-frequency noise, which is desirable since the feedback system will have appreciable gains at low frequency. The frequency spectrum of the light received by the photodiode during a plasma shot is shown in Figure 2-6.

The figure shows that most of the power in the light produced by the plasma is at

lower frequencies, as should be expected. At frequencies greater than ~30 kHz, the power carried is about 10000 times lower than the power carried by lower frequencies. So, with a sufficiently high modulation frequency, the signal to noise ratio for the received light signal should be about 1000000:1. At such a high ratio, the interference from the plasma light is a negligible effect in the noise characteristics of the system, and other sources of noise will be dominant.

2.2 Laser Emitter and Photodetectors

2.2.1 Development Work

Work on a homegrown laser position detector system was carried out over a period of time. The specifications called for a system that could measure displacements on the order of tens of microns over a distance of 5 meters with a field of view of several centimeters. A schematic of the system is shown in Figure 2-7. A modulated laser diode driver at 60 kHz was designed with feedback from an integral photodiode in the laser diode so that a constant power of laser light was emitted. This ensured that changes in the emission characteristics of the laser diode over time would not result in a change in the emitted power, which would appear to be a position drift at the detector side of the circuit. The diode driver was coupled to a fiber optic which had the fibers spread into a line at one end, providing a line source of laser light.

At the detector side, a lens was coupled to another fiber optic, which in turn fed the light to a photodiode. The signal from the photodiode was amplified and passed to a phase-locked loop, which produced a clean signal at the modulation frequency that was in phase with the received signal. This signal was mixed with the received signal from the photodiode, producing sum and difference signals. The result was low-pass filtered with a bandwidth of about 1kHz to isolate the signal that was originally within a 1kHz bandwidth of the modulation frequency.

This system design has the benefit that the laser source is shining directly at the photodetector, providing a larger signal to the photodector than a reflective measure-

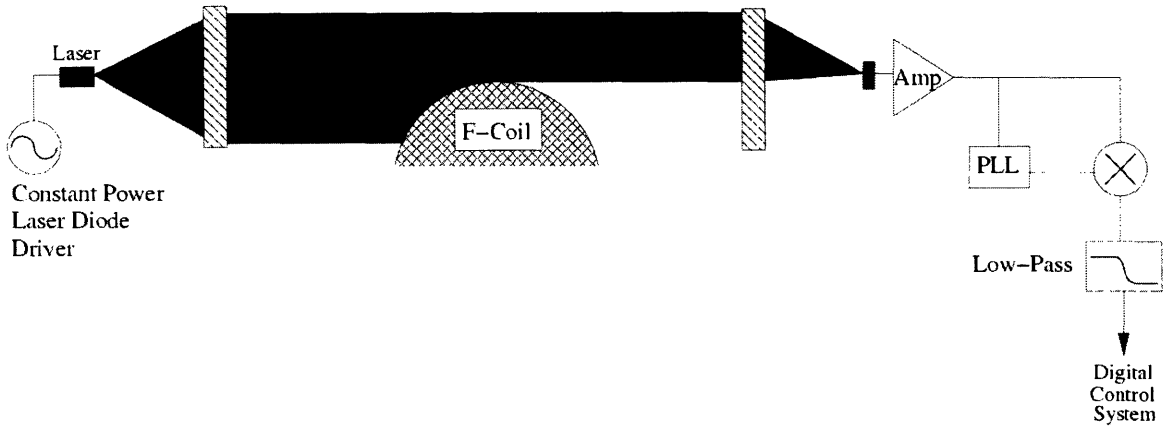

Figure 2-7: Schematic of the home-grown laser position detector system.

ment system might provide. This system can also be designed to be very sensitive to displacements, and is able to make measurements at a high frequency.

The system was developed to the point that it was able to work over about 2 meters of the 5 meter separation distance needed for the position detection system. The system was limited by optics which were not ideal for the application. This greatly decreased the transmission efficiency from the laser emitter to the detector. There was also some difficulty in tuning the phase-locked loop to correctly lock on to low-amplitude signals.

2.2.2 Commercial Solution

In the mean time, a newly developed commercially available system was found that meets the requirements for the position detection system. The Keyence LV-H300 [11] uses a wide, 3 centimeter laser beam pulsed at ~70 kHz and a similarly sized photodetector to measure the occlusion of the beam. This system is schematically identical to the homegrown solution, but with the PLL replaced by a reference signal from the modulator. The system has been demonstrated to measure changes in occlusion on the order of 10μm over the 5 meter length demanded of the position detection system. The Keyence system also has been demonstrated to measure events with a time scale of less than 100μs, so it will be able to provide information to the feedback system

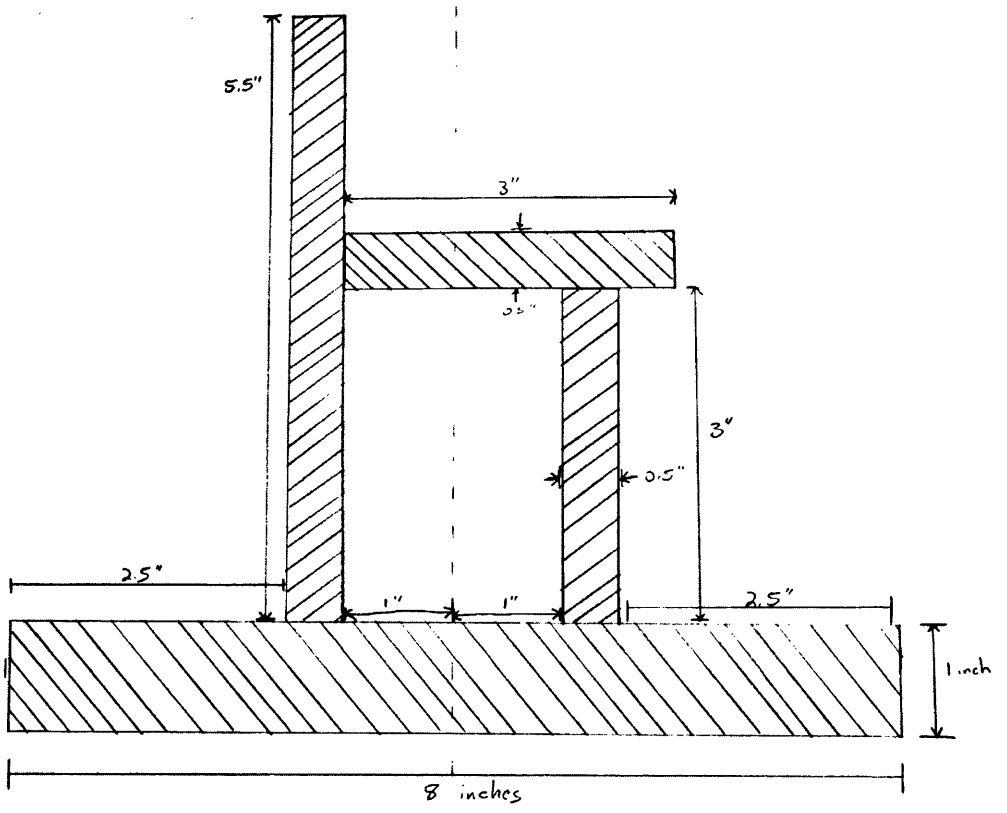

Figure 2-8: Side view of aluminum position detector support block.

at the desired frequency of 1 kHz.

2.3 Detector Mounting System

The detectors will be mounted in brackets provided by Keyence for use with their detectors. These brackets allow the position to be tuned in the vertical and horizontal directions. These brackets will be mounted on a support structure manufactured from aluminum as shown in Figures 2-8 and 2-9. One detector will be positioned horizontally and one vertically at each port to create the "L" shape needed to measure horizontal and vertical displacement at each point. The laser beams at each leg of the "L" will shine in opposite directions to avoid interference at the receiving end. The support structure will be positioned on top of rubber vibration-damping mounts, which will be in turn mounted on brackets attached to the side of the vacuum vessel.

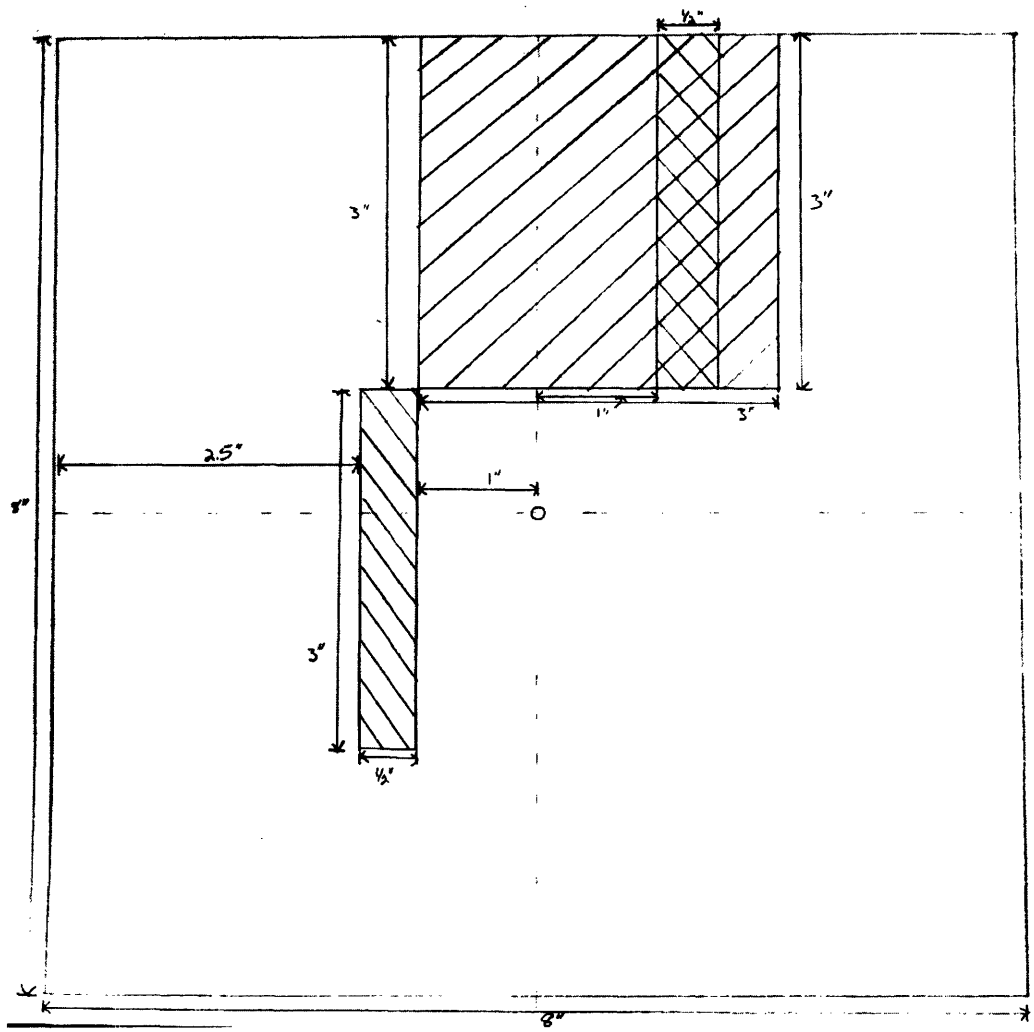

Figure 2-9: Top view of aluminum position detector support block.

2.4 Obtaining Vertical Position from Position Measurements

None of the measurements of the F-coil position is able to measure the displacement of one degree of freedom without taking into account the other measurements. In fact, the system is overconstrained, with eight measurements describing five degrees of freedom. This will allow one detector to be lost without compromising the system's ability to measure the F-coil position, allowing for the creation of a fault-tolerant control system at a later time.

For the first levitated operation, the measurement of interest will be the vertical position measurement. This measurement is determined by the received light from the vertical laser lines. These lines also carry information about the tilt of the coil, so it is necessary to process the information to separate the tilt and vertical displacement measurements.

If the measurements were made at the very end of the rim attached to the F-coil shown in Figure 2-2 , then it would be possible to simply take an average of the four vertical measurements in order to find the vertical displacement independently of the tilt. Such an arrangement is not possible, however, since a horizontal displacement could result in one of the laser lines disappearing off the edge of the rim and no longer carrying any information.

So, it is necessary for the beam to be moved in from the edge of the ring. Unfortunately, this creates a problem that the effects of coil tilt can no longer be removed simply by averaging the four measurements. Figure 2-10 shows the geometry with four inset measurements, Z_1, Z_2, Z_3, and Z_4. To see the problem, imagine that the coil is tilted about the axis labeled **B**. In this case, the measurements Z_1 and Z_3 will experience an equal and opposite displacement. However, Z_4 and Z_2 will both experience an offset in the vertical measurement because the laser intercepts a point of the ring which has been swung into the view of the laser because of the tilt. This offset is given by

$$\Delta Z_4 = \Delta Z_2 = \sqrt{R^2 - r^2}\cos\Theta_{\mathbf{B}} \tag{2.5}$$

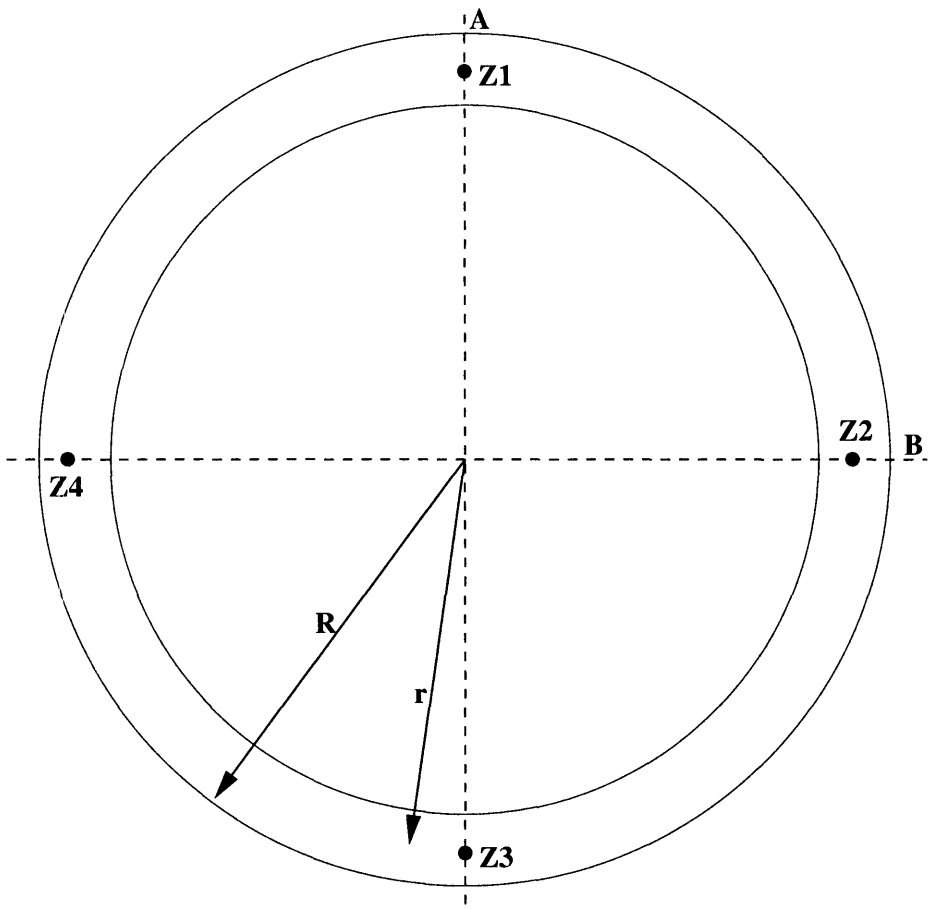

Figure 2-10: Overhead view of rim attached to F-coil and the four measurement points. **A** and **B** represent the two independent axes of tilt.

Here $\Theta_{\mathbf{B}}$ is the degree of tilt, R is the distance from the center of the F-coil to the edge of the rim, and r is the distance from the center of the F-coil to the point of measurement on the rim. This angle $\Theta_{\mathbf{B}}$ can be found from the measurements of Z_1 and Z_3 by

$$\cos\Theta_{\mathbf{B}} = \frac{|Z_1 - Z_3|}{2r} \tag{2.6}$$

A similar argument can be made for tilt about the **A** axis. With the tilt information, we can find the vertical displacement of the coil by averaging the four vertical displacement measurements minus the tilt-induced effects:

$$\begin{aligned} Z = \; & \tfrac{1}{4} \; [(Z_1 - \sqrt{R^2 - r^2}\cos\Theta_B) + (Z_2 - \sqrt{R^2 - r^2}\cos\Theta_A) \\ & + \; (Z_3 - \sqrt{R^2 - r^2}\cos\Theta_B) + (Z_4 - \sqrt{R^2 - r^2}\cos\Theta_A)] \\ \Rightarrow Z \; = \; & \frac{1}{4}\left[Z_1 + Z_2 + Z3 + Z4 - \sqrt{R^2/r^2 - 1}(|Z_1 - Z_3| + |Z_2 - Z_4|)\right] \end{aligned} \tag{2.7}$$

We can see that in the limit as $r \rightarrow R$, the displacement is simply the average of the four independent vertical position measurements as we would have expected.

Additional modifications to this formula can be made based on horizontal displacements, but the effects due to horizontal displacements are small corrections to the tilt-induced effects and are not included in this calculation.

Chapter 3

Digital Filters for the Position Measurements

As mentioned at the beginning of Chapter 2, noise reduction in the position measurements is important because of L-coil heating due to hysteresis losses when AC current is driven in the coil. Noisy measurements could create problems if the heating from the additional feedback exceeds the capacity of the L-coil refrigerator.

The feedback control of the F-coil is further complicated by non-linearities arising from frequency-dependent behavior of the L-coil and by interactions between the magnetic field and the supporting structure. In previous work in Reference [12], it was determined that digital Kalman filters were a candidate for filtering the received F-coil position measurements so that feedback may be applied to the L-coil power supply with as little heating of the L-coil as possible.

3.1 Overview of Digital Kalman Filtering

The Kalman filtering mechanism [13, 14] is a predictive corrective algorithm which proves to be very good at removing the noise in measurements, allowing the application of gains to relatively noise-free values.

A simple Kalman filter consists of a predictive step, in which the state variables for the current time step are predicted from past state variables, and a corrective

step, in which these values are corrected by taking into account the measurements at the current time step and estimations of noise. The following two steps make up the predictive part of the algorithm.

The vector $\mathbf{x_k}$ describes the state of the system at the timestep k. The matrix $\mathbf{A}$ describes how the state variables are expected to evolve assuming no driving of the system and no process noise, and $\mathbf{u_{k-1}}$ is a driving function. In general, $\mathbf{A}$ may be allowed to change as a function of time. The predicted evolution of the system is given by

$$\mathbf{x_k^*} = \mathbf{A}\mathbf{x_{k-1}} + \mathbf{u_{k-1}} \tag{3.1}$$

where $\mathbf{x_k^*}$ is the predicted value of $\mathbf{x}$ at the time step k. $\mathbf{A}$ and $\mathbf{u_{k-1}}$ are used to predict the evolution of the system, and are based on a physical understanding of the dynamics of the system.

The predicted estimate error covariance, $\mathbf{P^*}$ is given by

$$\mathbf{P_k^*} = \mathbf{A}\mathbf{P_{k-1}}\mathbf{A^T} + \mathbf{Q} \tag{3.2}$$

The estimate error covariance, $\mathbf{P}$, is representative of the deviations of the measurements from the internal state of the system. $\mathbf{Q}$, the process noise covariance, is a user-definable parameter that describes the uncertainty in the model of the system.

Before we show the equations of the corrective part of the algorithm, we need to define the the quantity $\mathbf{H}$ by

$$\mathbf{z_k} = \mathbf{H}\mathbf{x_k} + \mathbf{v_k} \tag{3.3}$$

Here, the internal state of the system is $\mathbf{x_k}$, $\mathbf{v_k}$ is random noise, and $\mathbf{z_k}$ is a measurement that is input into the system. So, $\mathbf{H}$ describes the relationship between the measurements taken and the state variables of the system.

Now we can examine the equations for the corrective part of the Kalman filtering algorithm.

First, the Kalman Gain, $\mathbf{K_k}$ is calculated by

$$\mathbf{K_k} = \mathbf{P_k^* H^T (H P_k^* H^T + R)^{-1}} \tag{3.4}$$

where $\mathbf{R}$ is the measurement noise covariance matrix. This is a measure of the expected noise in the system, and can be tuned to obtain the best performance for the filter. A good estimate for this value can be obtained by examining the noise in the measurements during calibration.

After the computation of the Kalman gain, the estimates $\mathbf{x_{k+1}^*}$ and $\mathbf{P_{k+1}^*}$ are updated, providing the Kalman-filtered state variables

$$\mathbf{x_k} = \mathbf{x_k^* + K_k(z_k - Hx_k^*)} \tag{3.5}$$

$$\mathbf{P_k} = \mathbf{(I - K_k H)P_k^*} \tag{3.6}$$

3.2 Implementing Kalman Filters for the Levitation Control System

Since it has been decided that Kalman filtering is a candidate for the levitation control system digital filtering algorithm, it is desirable to implement a Kalman filtering algorithm to run in the real-time operating system.

Using a suite of software named Opal-RT[9], code written in MATLAB Simulink can be translated into C code and compiled on the computer running QNX. The Kalman filtering algorithm was written in MATLAB Simulink, and a basic model of the floating coil dynamics was also programmed in order to test the filtering algorithm and the feedback.

3.2.1 A Basic Model of F-coil Dynamics

In order to test the Kalman filtering algorithm, a basic model of the F-coil dynamics was programmed in MATLAB Simulink. This model, developed in References [15]

and [16], is a simple model of the vertical response of the F-coil around its equilibrium position:

$$\frac{dz}{dt} = v_z \tag{3.7}$$

$$\frac{dv_z}{dt} = g(i_l - 1) + \gamma^2 z \left(1 + \frac{z}{d_{z1}} + \left(\frac{z}{d_{z2}}\right)^2 + \left(\frac{z}{d_{z3}}\right)^3\right) \tag{3.8}$$

$$\frac{di_l}{dt} = \frac{V}{L_l I_o} \tag{3.9}$$

Here the acceleration of the of the F-coil is given in terms of g, which is acceleration due to gravity, i_l, which is the levitation field normalized to $I = I_o$, the equilibrium L-coil current, and the expansion of the field to third order about the equilibrium z-coordinate, where γ =3.8 s^{-1} and $(d_{z1}, d_{z2}, d_{z3}) = (51, 82, 86)$ cm. The time derivative of the normalized field is given in terms of $L_l I_o = 680\,\mathrm{V}\cdot\mathrm{s}$ and the voltage applied to the L-coil, V.

This model provides a reasonable approximation of the F-coil dynamics and is useful for testing the Kalman filtering algorithm. However, this model does leave out several features of the levitation system dynamics. This model does not include effects due to eddy currents in the L-coil supports and the vacuum vessel. It doesn't include effects due to the frequency-dependent response of the L-coil. It also does not represent the flux-conserving nature of the F-coil; however, this creates only a small change in the forces since the mutual inductance between the L-coil and F-coil is much smaller than the inductance of the F-coil.

3.2.2 Kalman Filters for the Levitation Control System

For the levitation control system, we implement the Kalman filters in the following way as suggested in Reference [12]:

The state vector $\mathbf{x_k}$ is simply a vector of the current vertical F-coil position and

the position from two previous time steps:

$$\mathbf{x_k} = \begin{pmatrix} z_k \\ z_{k-1} \\ z_{k-2} \end{pmatrix} \tag{3.10}$$

Here the matrix $\mathbf{H}$ takes on a particularly simple form. Since our measurements correspond directly to the state quantities, $\mathbf{H} = \mathbf{I}$. This means that the Kalman filter equations reduce to

$$\mathbf{x_k^*} = \mathbf{A} \cdot \mathbf{x_{k-1}} + \mathbf{u_k} \tag{3.11}$$

$$\mathbf{P_k^*} = \mathbf{A} \cdot \mathbf{P_{k-1}} \cdot \mathbf{A^T} + \mathbf{Q} \tag{3.12}$$

$$\mathbf{K_k} = \mathbf{P_k^*} \cdot (\mathbf{P_k^*} + \mathbf{R})^{-1} \tag{3.13}$$

$$\mathbf{x_k} = \mathbf{x_k^*} + \mathbf{K_k} \cdot (\mathbf{z_k} - \mathbf{x_k^*}) \tag{3.14}$$

$$\mathbf{P_k} = (\mathbf{I} - \mathbf{K_k}) \cdot \mathbf{P_k^*} \tag{3.15}$$

The predicted evolution of the system is given by

$$\mathbf{x_k^*} = \begin{pmatrix} \gamma^2\delta t^2 + 2 & -1 & 0 \\ 1 & 0 & 0 \\ 0 & 1 & 0 \end{pmatrix} \cdot \begin{pmatrix} z_{k-1} \\ z_{k-2} \\ z_{k-3} \end{pmatrix} + \begin{pmatrix} g\delta t^2(i_l(k-1) - 1) \\ 0 \\ 0 \end{pmatrix} = \mathbf{A} \cdot \mathbf{x_{k-1}} + \mathbf{u_{k-1}} \tag{3.16}$$

where $i_l(k-1)$ is the measured normalized current in the L-coil during the time-step $k-1$.

With the filtered measurements of the F-coil position, we can then apply gains based on the calculated position, velocity and acceleration of the F-coil

$$V_k = (G_p \; G_d \; G_{d2}) \cdot \begin{pmatrix} 1 & 0 & 0 \\ 1/\delta t & -1/\delta t & 0 \\ 1/\delta t^2 & -2/\delta t^2 & 1/\delta t^2 \end{pmatrix} \cdot \mathbf{x_k} \tag{3.17}$$

Here we have applied a proportional gain and gains based on the calculated discrete

first and second derivatives, similar to a PID loop controlling i_l.

3.3 Testing the Filtering Algorithm

The Kalman filtering algorithm and the simple F-coil dynamics model were implemented in MATLAB Simulink, which is the desired development environment for the levitation control system. Random noise with an amplitude of 0.1 millimeters was added to the position calculated from the F-coil dynamics model, and this signal was passed to the Kalman filtering algorithm. The values of the noise covariances were taken to be $\mathbf{R} = \mathbf{40000} * \mathbf{I}$ and $\mathbf{Q} = \mathbf{0.001} * \mathbf{I}$. The measurement noise covariance $\mathbf{R}$ is taken to be high because of the relatively high random noise added to the system, while the process noise covariance $\mathbf{Q}$ is taken to be low since the Kalman filter's internal state model very accurately describes the simulated dynamics of the system. The gains were taken to be $(G_p\ G_{d1}\ G_{d2}) = (-1.0, -12, -1.7)$. At time t=0 the F-coil was given an upward push at a velocity 1 cm/sec, and the resulting response of the system is shown in Figures 3-1 and 3-2.

This resulted in good control of the F-coil, and the extraneous voltage applied to the L-coil in response to noise was kept slightly below 1 volt. Evaluating the phase delay reveals some slightly troubling behavior. Although the Kalman-filtered displacement measurement closely matched the true value during almost all of the simulation as shown in Figure 3-3, at the start of the simulation the values separated significantly as shown in Figure 3-4.

This result is not particularly surprising. When the simulation is run with a large measurement noise covariance, the filter does quite well at rejecting noise. Unfortunately, it is slow to respond to changes in the system. After the initial discontinuity in the dynamics with the kick start at t=0, the filter is eventually able to lock on to the true position. From that point on, there is an immeasurably small phase delay since the expected evolution of the system from the Kalman filter's point of view is exactly the evolution of the system programmed into the dynamics simulator.

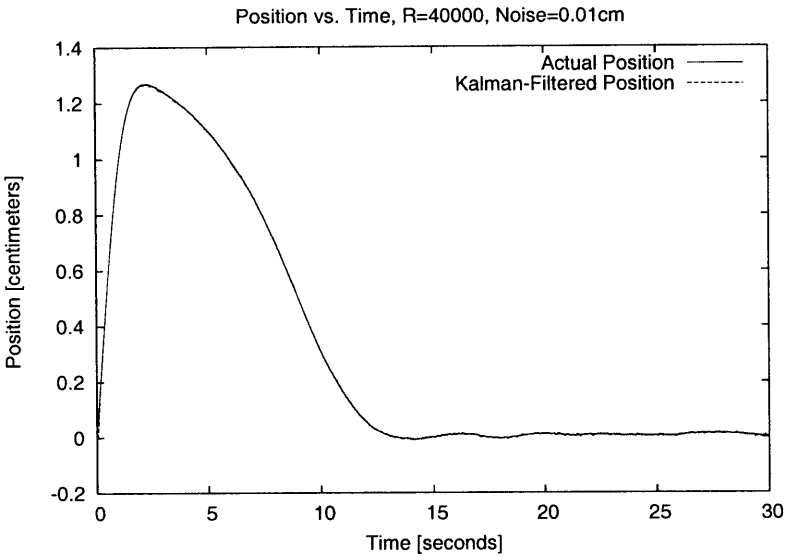

Figure 3-1: Actual vertical displacement and Kalman-filtered displacement in the vertical position.

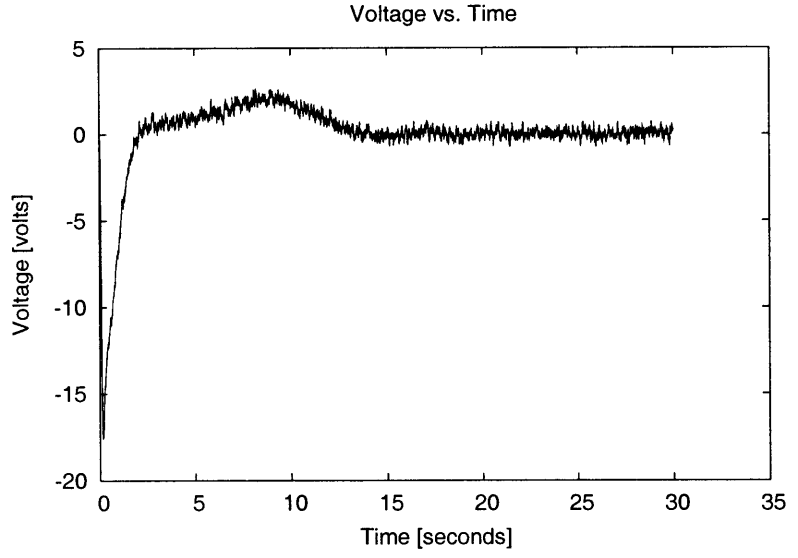

Figure 3-2: Voltage applied to the L-coil in the model of the F-coil dynamics.

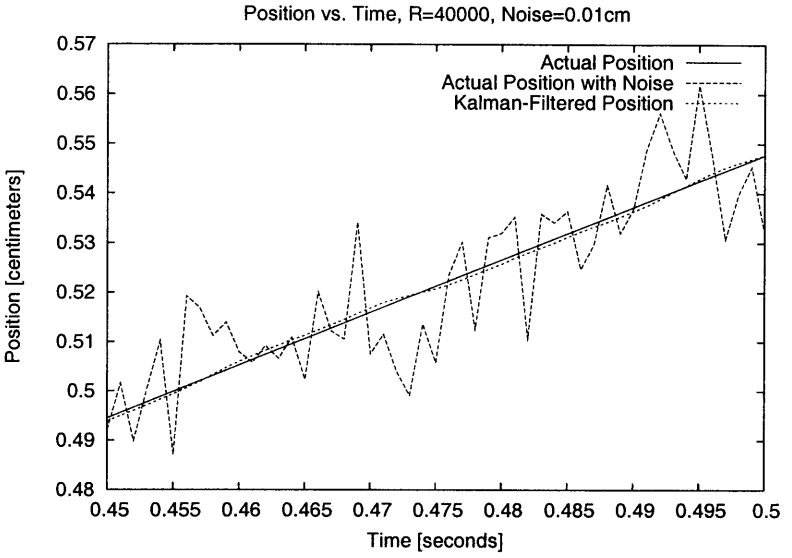

Figure 3-3: Plot showing the Kalman filtered position measurement and the true position measurement at one point during the simulation. There is almost no phase delay, as was the case for most of the simulation.

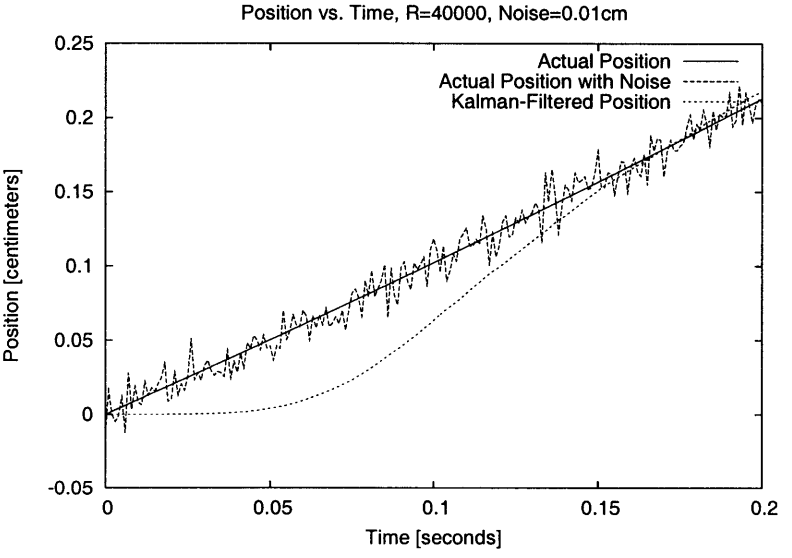

Figure 3-4: Plot showing the Kalman filtered position measurement and the true position measurement at the start of the simulation. There is significant phase delay.

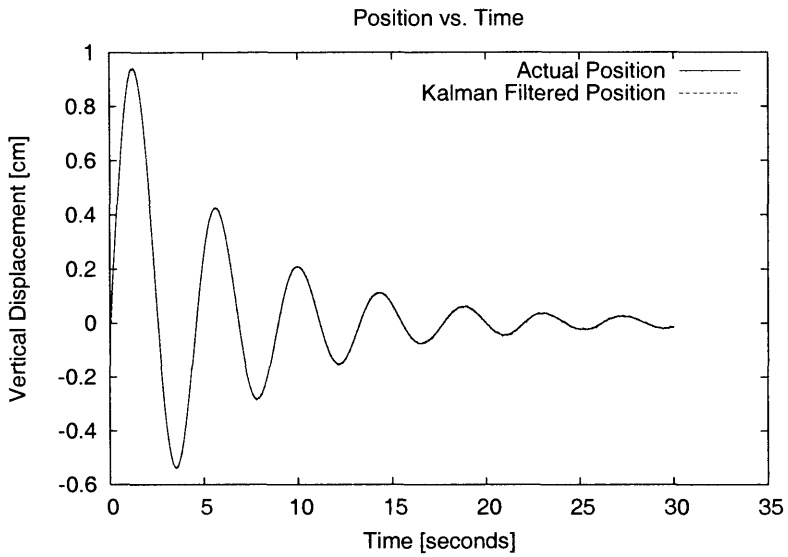

Figure 3-5: Actual vertical displacement and Kalman-filtered displacement in the vertical position with $\mathbf{R} = \mathbf{40000I}$ and $\mathbf{u} = \mathbf{0.95u}$.

3.3.1 Detuning the Kalman Filter

In the last simulation, the Kalman filter got off easy by having a perfect representation of the F-coil dynamics programmed into its state evolution equation. In this simulation, the state evolution equations were slightly detuned by multiplying the vector $\mathbf{u_{k-1}}$ by 0.95, and the noise covariances were unchanged. This created a disparity between the actual evolution of the model and the evolution that the Kalman filter expected.

The results of the control are shown in Figures 3-5 and 3-6. The F-coil was still controlled, but it is clearly underdamped. The voltage due to noise fluctuations was still kept under 1 Volt. In Figure 3-7 we can see that there was still significant phase delay at the start of the simulation. We also see a delay on the order of about 3 ms in the middle of the simulation, as shown in Figure 3-8.

We can begin to see the tradeoffs between filter phase delay and noise suppression that will need to be made in the ultimate design of the Kalman filters. In situations where the Kalman filter's expected evolution of the system exactly matches physical reality, it is possible to have both high noise suppression and no phase delay. However, it would be very difficult to give a full physical description of the dynamics to the

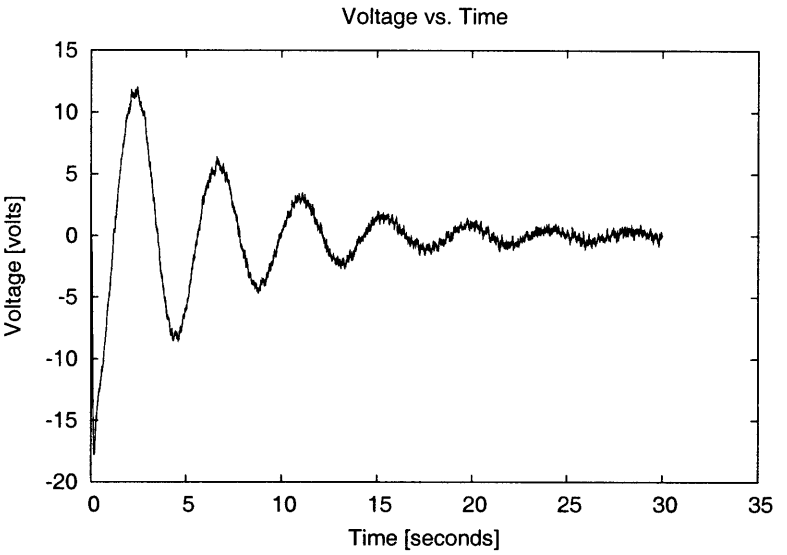

Figure 3-6: Voltage applied to the L-coil in the model of the F-coil dynamics with $\mathbf{R} = \mathbf{40000I}$ and $\mathbf{u} = \mathbf{0.95u}$.

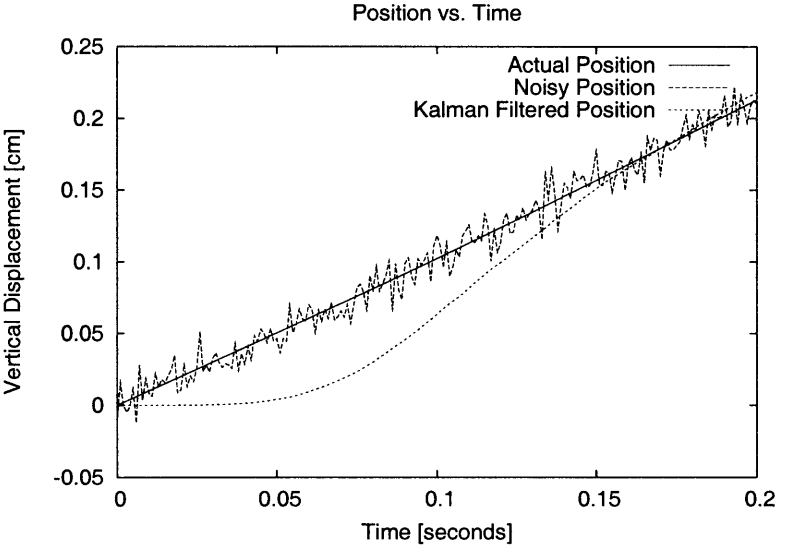

Figure 3-7: Plot showing the Kalman filtered position measurement and the true position measurement at the start of the simulation with $\mathbf{R} = \mathbf{40000I}$ and $\mathbf{u} = \mathbf{0.95u}$.

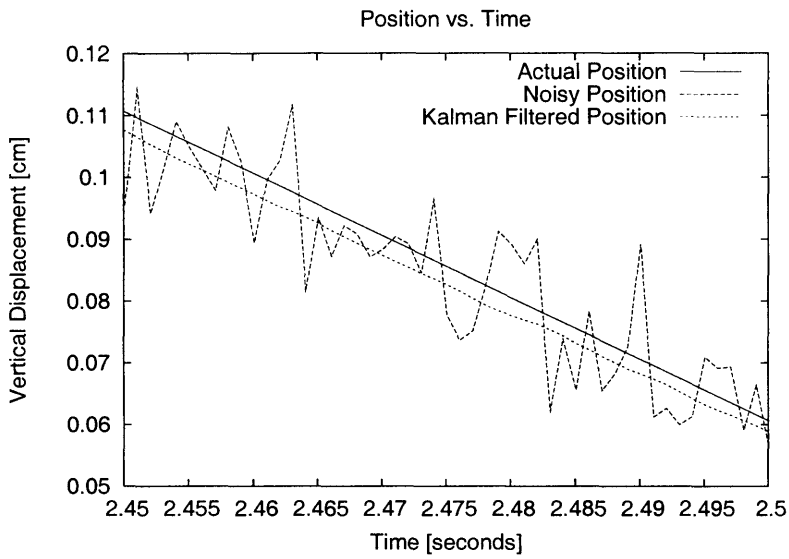

Figure 3-8: Plot showing the Kalman filtered position measurement and the true position measurement at one point during the simulation with $\mathbf{R} = \mathbf{40000I}$ and $\mathbf{u} = \mathbf{0.95u}$.

filter, and thus a tradeoff in the filter performance will have to be made. It may be advantageous to investigate more advanced control algorithms that are able to dynamically adapt the expected state evolution equations in order to minimize the phase delay caused by imperfect equations.

Chapter 4

Conclusions and Future Work

4.1 Summary

In this thesis a design of the floating coil position detection system for the Levitated Dipole Experiment was presented and justified. The system consists of commercially available modulated laser position sensors that are able to measure displacements of the F-coil on the order of tens of microns across the five meter vacuum vessel at a high frequency while rejecting ambient light noise. These sensors provide the position information to a feedback system consisting of a PC running a hard real-time operating system, which applies digital Kalman filters to the position information to which gains can be applied to control the current in the levitation coil.

4.2 Future Work

While many of the individual components in the levitation control system have been designed, the final construction and integration of the components needs to be performed. The steps involve:

- Installing and calibrating the position detection sensors
- Wiring the position detection sensors to the feedback-controlling computer

- Integrating the output from the feedback-controlling PC with the L-coil power supply
- Testing the system as a whole to adjust the values of the feedback gains
- Investigating other modern optimal control system designs to minimize hysteresis losses in the L-coil

Additional work may need to be done to control the damping of the stable modes of oscillation of the system. Stabilizing the vertical position of the coil is the first goal in the levitation, since the levitation cannot occur without the feedback-provided stability. However, the experimental goals may require that the other modes be damped. This would require additional feedback paths to determine the voltages to be applied to a set of controlling coils on the outside of the vacuum vessel.

Bibliography

[1] M. MAUEL D. GARNIER J. KESNER, L. BROMBERG and J.M. DAWSON. The Dipole Fusion Confinement Concept: A White Paper for the Fusion Community. 1998. Available online at `http://www.psfc.mit.edu/ldx/pubs/dipole_fesac.pdf`.

[2] J. KESNER and D.T. GARNIER. Convective Cell Formation in a Levitated Dipole. *Phys. Plasmas*, 7:2733, 2000. Available online at `http://www.psfc.mit.edu/ldx/pubs/kesner_pop00.pdf`.

[3] A. HANSEN M. MAUEL J. KESNER, D.T. GARNIER and L. BROMBERG. D-D Fusion in a Levitated Dipole. *Nuclear Fusion*, 44:193, 2004. Available online at `http://www.psfc.mit.edu/ldx/pubs/DD_ldr_v3.pdf`.

[4] S. EARNSHAW. On the nature of the molecular forces which regulate the constitution of the luminiferous ether. *Trans. Camb. Phil. Soc.*, 7:97, 1842.

[5] J.D. JACKSON. *Classical Electrodynamics.* Wiley, 3 edition, Hoboken, NJ.

[6] M.V. BERRY and A.K. GEIM. Of flying frogs and levitrons. *Eur. J. Phys*, 18:307–313, 1997. Available online at `http://stacks.iop.org/0143-0807/18/307`.

[7] QNX Software Systems, Ottawa, Ontario, Canada. `http://www.qnx.com`.

[8] The Mathworks, Inc., Natick, Massachusetts. `http://www.mathworks.com`.

[9] Opal-RT Technologies, Inc., Montreal, Quebec, Canada. `http://www.opal-rt.com`.

[10] W.J. CARR JR. *AC Loss and Macroscopic Theory of Superconductors.* Gordon and Beach, New York, 1983.

[11] Keyence Corporation of America, Woodcliff Lake, New Jersey. `http://www.keyence.com`.

[12] M.E. MAUEL. Feedback Control Update. Memo to LDX Group, April 2004.

[13] C.K. CHUI and G. CHEN. *Kalman Filtering with Real Time Applications.* Springer-Verlag, New York, 2nd edition, 1991.

[14] G. WELCH and G. BISHOP. An Introduction to the Kalman Filter. Accessed Online April 2005 at `http://www.cs.unc.edu/~welch/media/pdf/kalman_intro.pdf`, April 2004.

[15] T.S. PERDERSEN et al. Computer simulations and design of levitation feedback control system for LDX. *APS Division of Plasma Physics Meeting.*

[16] T.S. PEDERSEN. LDX Feedback Control Simulations with Noise. 2001. Memo LDX-CU-TSP-120800-01.